



Article

Xenophyllite, $\text{Na}_4\text{Fe}_7(\text{PO}_4)_6$, an Exotic Meteoritic Phosphate: New Mineral Description, Na-ions Mobility and Electrochemical Implications

Sergey N. Britvin ^{1,2,*} , Sergey V. Krivovichev ^{1,2}, Edita V. Obolonskaya ³, Natalia S. Vlasenko ⁴, Vladimir N. Bocharov ⁴  and Vera V. Bryukhanova ⁵

¹ Department of Crystallography, Institute of Earth Sciences, St. Petersburg State University, Universitetskaya Nab. 7/9, 199034 St. Petersburg, Russia; skrivovi@mail.ru

² Nanomaterials Research Center, Kola Science Center of Russian Academy of Sciences, Fersman Str. 14, 184209 Apatity, Russia

³ The Mining Museum, Saint Petersburg Mining University, 2, 21st Line, 199106 St. Petersburg, Russia; musmet11@yandex.ru

⁴ Centre for Geo-Environmental Research and Modelling, Saint-Petersburg State University, Ulyanovskaya ul. 1, 198504 St. Petersburg, Russia; ly17@mail.ru (N.S.V.); bocharov@molsph.phys.spbu.ru (V.N.B.)

⁵ Interdisciplinary Resource Centre for Nanotechnology, Saint-Petersburg State University, Ulyanovskaya ul. 1, 198504 St. Petersburg, Russia; v.bryukhanova@spbu.ru

* Correspondence: sergei.britvin@spbu.ru

Received: 29 February 2020; Accepted: 25 March 2020; Published: 27 March 2020



Abstract: Xenophyllite, ideally $\text{Na}_4\text{Fe}_7(\text{PO}_4)_6$, is a rare meteoritic phosphate found in phosphide-phosphate assemblages confined to troilite nodules of the Augustinovka iron meteorite (medium octahedrite, IIIAB). The mineral occurs as tiny lamella up to 0.15 mm long cross-cutting millimeter-sized grains of sarcopside, $\text{Fe}_3(\text{PO}_4)_2$, associated with schreibersite, chromite and pentlandite. Xenophyllite is translucent, has a bluish-green to grey-green color and vitreous lustre. Moh's hardness is 3.5–4. Cleavage is perfect on {001}. Measured density is $3.58(5) \text{ g/cm}^3$. The mineral is biaxial (–), $2V$ $10\text{--}20^\circ$, with refractive indexes: α 1.675(2), β 1.681(2), γ 1.681 (2). Chemical composition of the holotype specimen (electron microprobe, wt.%) is: Na_2O 10.9, K_2O 0.4, MnO 5.8, FeO 42.1, Cr_2O_3 0.8, P_2O_5 40.7, total 100.7, corresponding to the empirical formula $(\text{Na}_{3.67}\text{K}_{0.09})_{\Sigma 3.76}(\text{Fe}^{2+}_{6.12}\text{Mn}^{2+}_{0.85}\text{Cr}_{0.11})_{\Sigma 7.08}\text{P}_{5.99}\text{O}_{24.00}$. Xenophyllite is triclinic, $P1$ or $P-1$, a 9.643(6), b 9.633(5), c 17.645(11) Å; α 88.26(5), β 88.16(5), γ 64.83(5)°, V 1482(2) Å³, Z = 3. The toichiome C-centered subcell has the following dimensions: a 16.257(9), b 10.318(8), c 6.257(9) Å, β = 112.77(9)°, V 968(2) Å³, Z = 2. Xenophyllite is structurally related to synthetic phosphate $\text{KNa}_3\text{Fe}_7(\text{PO}_4)_6$ having a channel-type structure, and galileiite, $\text{NaFe}_4(\text{PO}_4)_3$. The variations of chemical composition of xenophyllite ranging from $\text{Na}_4\text{Fe}_7(\text{PO}_4)_6$ to almost $\text{Na}_2\text{Fe}_8(\text{PO}_4)_6$ are accounted for by Na-ions mobility. The latter property makes xenophyllite a promising prototype for cathode materials used in sodium-ion batteries.

Keywords: xenophyllite; new mineral; iron phosphate; meteorite; galileiite; cathode; cation mobility; sodium-ion batteries

1. Introduction

The discoveries of new functional materials have often been inspired by the study of their natural counterparts. Phosphate mineral triphylite, LiFePO_4 (the olivine structure type) [1] is among those prototypes whose structural motif has led to an emergence of a novel class of cathodes for lithium-ion batteries [2,3]. Meanwhile, the growing demand for inexpensive electrochemical energy sources has resulted in the development of Na-ion batteries which require novel electrode materials based on

fast and stable Na-ion conductors [4]. We herein provide the first mineralogical characterization, X-ray investigation and chemistry of a new meteoritic mineral xenophyllite, $\text{Na}_4\text{Fe}_7(\text{PO}_4)_6$, whose synthetic analogue was recently offered as a promising candidate for cathode materials in sodium-ion batteries [5]. Xenophyllite was discovered in the course of a study of phosphide-phosphate assemblages confined to troilite nodules of the Augustinovka iron meteorite (medium octahedrite, IIIAB), and was named from Greek ξένος (xénos, stranger) and φύλλο (fýllo, leaf), for its extraterrestrial origin and perfect cleavage of its crystals. Both the mineral and the name have been approved by the Commission on New Minerals and Mineral Names, International Mineralogical Association [6]. The holotype specimen of xenophyllite is deposited at the collection of the Mining Museum, Saint Petersburg Mining University, St. Petersburg, Russia, under the inventory number 23/2005.

2. The Augustinovka Meteorite

The Augustinovka is an iron meteorite belonging to medium-structure octahedrites (Om) and related to a chemical group IIIA. A single mass weighted about 400 kg was recovered in 1890 on the left bank of the Dnepr river, nearby the Augustinovka village, Jekaterinoslav District, Russia (later on Dnepropetrovsk District, Ukrainian S.S.R., U.S.S.R., now belonging to Zaporizhia District, Ukraine) (48°4' N, 35°5' E) [7,8]. The whole mass has been transported to the Mining Institute in Saint-Petersburg where a few pieces were cut off for the study and distribution among the museums. The 276 kg main mass is now stored at the meteoritic collection of the Mining Museum, Saint Petersburg Mining University. A mineralogical and metallographic description of the meteorite is given by Buchwald [9] who mentioned the enrichment of the Augustinovka in centimeter-sized troilite nodules of nearly spherical shape, which are clearly visible at the front cut of the main meteorite mass [10]. Millimeter-sized phosphate inclusions in troilite from the Augustinovka were first encountered by Olsen and Fredriksson [11,12] who identified them as being composed of sarcopside, $(\text{Fe,Mn})_3(\text{PO}_4)_2$, with minor amounts of Ca-free graffonite (the latter mineral is now classified as graffonite-(Mn) [13]).

3. Materials and Methods

Several cm-sized fragments of troilite nodules from the Augustinovka were kindly provided for the present study by the Mining Museum, Saint Petersburg Mining University, Saint Petersburg, Russia. The fragments were shred into ~1 mm thick slices which were used for a further preparation of the polished thin sections. The sections were first examined under a polarizing microscope in reflected and transmitted light. After that, selected sections containing phosphate grains were coated with conductive carbon film and subjected to the electron microprobe study. Because of instability (quick loss of sodium) of xenophyllite under the conditions of wavelength-dispersive (WDX) analysis, the chemical composition of the mineral and associated phases was studied in energy-dispersive mode (EDX) by means of an Oxford Instruments CamScan 4 scanning electron microscope (Abingdon, UK) equipped with a LINK AN1000 EDS detector, under 20 kV accelerating voltage, 1 nA beam current, 3 µm beam diameter and 30 s counting time per spot. Analytical standards used were chkalovite (for Na), orthoclase (K), diopside (Mg), metallic Mn and Co (Mn and Co), hematite (Fe), chromite (Cr), chlorapatite (P), and pyrite (S). The microprobe data were processed using the built-in Oxford Instruments software using a conventional ZAF procedure. The analyses of associated minerals were performed by use of an AzTec Energy X-Max 20 EDX spectrometer (AzTec Energy Group Inc., Brentwood, NY, USA) attached to a Hitachi S-3400N scanning electron microscope (SEM) (Hitachi, Ltd., Tokyo, Japan). EDX spectra were obtained using 20 kV accelerating voltage, 2 nA beam current, and 60 s acquisition time per spectrum, and were processed using ZAF. The density of xenophyllite was measured on the isolated grain by sink-float method in the diluted Clerici solutions. X-ray single-crystal data were obtained from the $0.05 \times 0.05 \times 0.05$ mm grain extracted from a polished section, by means of a STOE IPDSII imaging plate diffractometer (STOE & Cie GmbH, Darmstadt, Germany) ($\text{MoK}\alpha$ -radiation, 50 kV, 40 mA, detector-to-crystal distance 100 mm). A set of 90 frames (0–180°) was collected using ω -scan (2° frame width and 300 s exposure time per frame). Data processing and unit-cell parameters determination was

performed by means of STOE X-area v.1.42 software (STOE & Cie GmbH, Darmstadt, Germany) [14]. X-ray powder diffraction pattern (Figures S1 and S2) was obtained using a Gandolfi method by means of a Rigaku RAXIS Rapid II diffractometer (Rigaku Corporation, Tokyo, Japan) equipped with a semi-cylindrical imaging plate and operated under the following setup: CoK α -radiation (rotating anode with microfocus optics), 40 kV acceleration voltage, 15 mA tube current, 127.4 mm detector-to-crystal distance and 60 min overall exposure time. Subsequent powder X-ray diffraction (XRD) data processing and unit-cell parameters refinement was performed using an osc2xrd and STOE WinXPOW v. 1.06 software [15,16]. The Raman spectrum of xenophyllite was recorded by means of a Horiba Jobin-Yvon LabRam HR 800 spectrometer (Horiba Scientific, Kyoto, Japan) equipped with a 514 nm Ar⁺ laser and 50 \times confocal objective focused to 2 μ m spot size. The output power of a laser was reduced by 30% to ~13 mW (~1 mW on sample), in order to avoid radiation-induced damage of the mineral detected during the screening measurements.

4. Results

4.1. Occurrence and Associated Minerals

Xenophyllite is a rare mineral hosted within millimeter-sized phosphate-phosphide assemblages confined to centimeter-sized ovoidal troilite nodules common in the Augustinovka meteorite. Troilite has a fine-grained lenticular texture revealed under crossed polars (Figure 1a). The dominant phase among phosphates is sarcopside, which forms pseudo-euhedral grains reaching up to 3 mm disseminated in troilite (Figure 1). Macroscopically, sarcopside is translucent; the fresh mineral has a grayish color but it is frequently dissected by the submicroscopic web of secondary vivianite veinlets which impart the pale- to deep-blue color to sarcopside grains. Although sarcopside often exhibits very sharp euhedral faces (Figure 1a), examination in transmitted light under crossed polars (Figure 1b) always reveals very complex mosaic structure; thus the observed faces do not correspond to sarcopside single crystals in its present state. The mineral grains commonly consist of complex polysynthetic twins (Figure 1c). Sometimes, sarcopside grains are severely fragmented (Figure 1d) and even dissected by the late troilite veinlets (Figure 1e). Sarcopside is frequently enveloped by the rims composed of fine-grained intergrowths of chromite and schreibersite (Figure 1e). In the course of powder X-ray examination of phosphate assemblages of Augustinovka, we only detected sarcopside itself, with no evidence of graffonite previously mentioned by Olsen and Fredriksson [11]. The unit-cell parameters of sarcopside (space group $P2_1/c$) are: a 10.554(9), b 4.748(5), c 6.054(3) Å, β 91.09(8)°. The mineral is very uniform in chemical composition and has no compositional zoning; it contains 1.7 to 2.6 wt.% MnO (Table 1).

Chromite (Figure 1e) approaches nearly pure end-member (Table 1). Schreibersite (Figure 1e) exhibits almost constant Fe/Ni ratio (Table 2). Troilite is a pure stoichiometric FeS. The composition of pentlandite could not be accurately determined because its tiny (1–2 μ m thick) veinlets interfere with encasing troilite; semi-quantitative determinations show Ni contents up to 30 wt.%.

Table 1. Chemical composition of sarcopside and chromite from troilite nodules of the Augustinovka meteorite.

	Sarcopside			Chromite		
	wt.% ¹	Range	sd ³	wt.% ²	Range	sd ³
FeO	57.30	56.51–57.72	0.33	32.01	31.44–32.66	0.43
MnO	2.12	1.72–2.61	0.23	0.20	0.00–0.56	
CoO	0.08	0.00–0.25		0.16	0.00–0.42	
Cr ₂ O ₃	bdl ⁴			68.03	67.47–68.47	0.40
P ₂ O ₅	40.19	39.80–40.60	0.20	bdl ⁴		
Total	99.69			100.40		

¹ Average of 18 analyses on 6 grains. Empirical formula recalculated on 8 oxygen atoms per formula unit: (Fe_{2.84}Mn_{0.11})_{2.95}P_{2.02}O₈. ² Average of 6 analyses on 3 grains. Empirical formula recalculated on 4 oxygen atoms per formula unit: (Fe_{0.99}Mn_{0.01})_{1.00}Cr_{2.00}O₄. ³ Standard deviation (sd). ⁴ Below detection limit (bdl) (~0.05 wt.%).

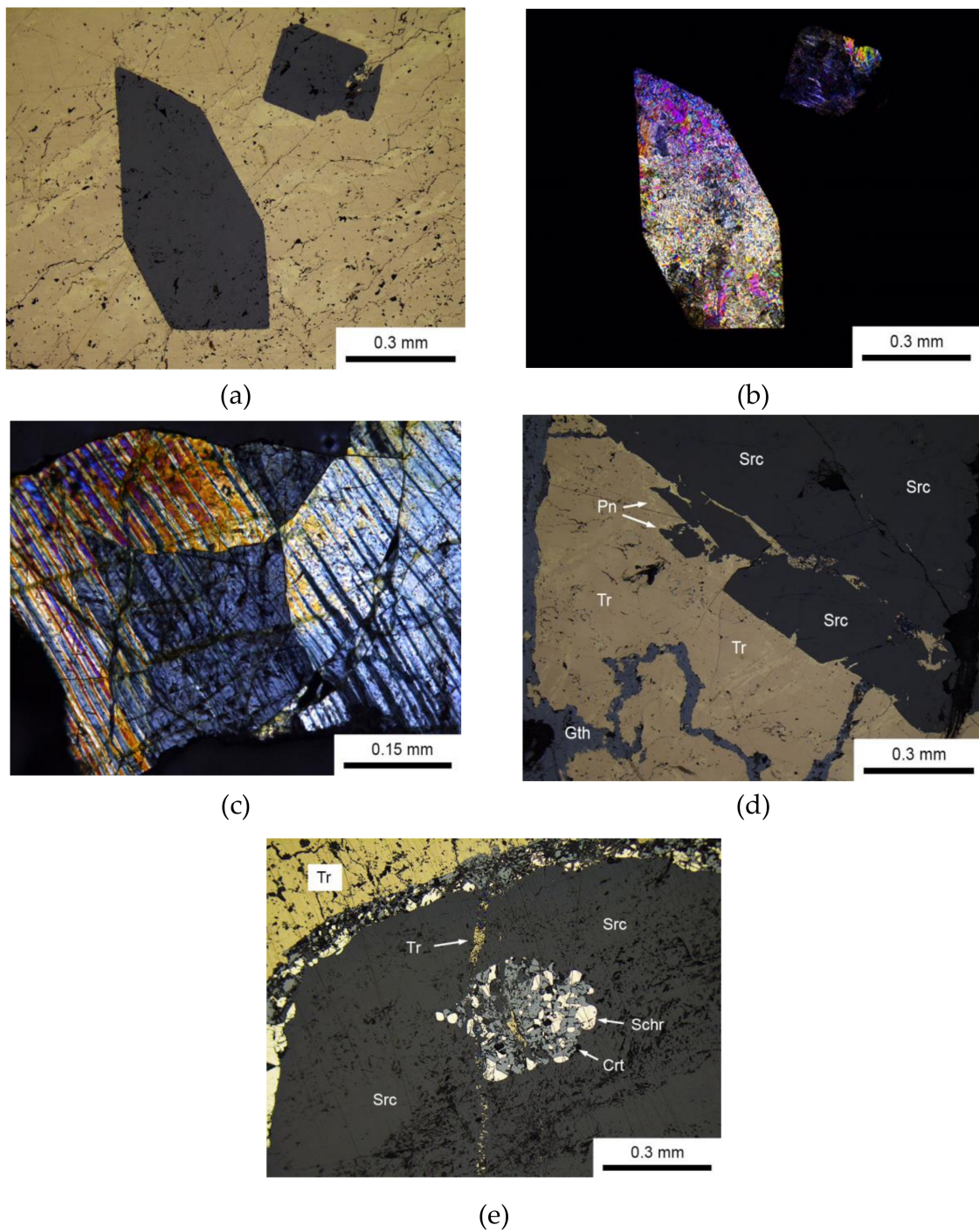


Figure 1. Phosphate-phosphide assemblages of troilite nodules of the Augustinovka meteorite. (a) Pseudo-euhedral sarcopside grains (dark-grey) in fine-grained troilite. The lenticular structure of host troilite is revealed by color variations in yellow-tan hues. Reflected light, crossed polars. (b) The same area in transmitted light under crossed polars. Note the mosaic interior of macroscopically euhedral sarcopside crystals. (c) Polysynthetic twinning typical of sarcopside from Augustinovka. Transmitted light, crossed polars. (d) Brecciated sarcopside grain surrounded by pentlandite veinlets in partially altered troilite. Reflected light, crossed polars. (e) Sarcopside grain penetrated by the troilite veinlet, enveloped in and hosting fine-grained chromite-schreibersite aggregates. Reflected light, parallel polars. Abbreviations: Src, sarcopside; Tr, troilite; Pn, pentlandite; Schr, schreibersite; Crt, chromite; Gth, goethite (weathering product). Photomicrographs by Sergey Britvin.

Table 2. Chemical composition of schreibersite from troilite nodules of the Augustinovka meteorite.

	Wt.% ¹	Range	sd ²
Fe	62.17	61.15–63.39	0.78
Ni	22.18	21.29–23.14	0.76
Co	0.19	0.13–0.27	0.05
P	15.51	15.30–15.85	0.17
S	bdl ³		
Total	100.05		

¹ Average of 12 analyses on 6 grains. Empirical formula recalculated on 4 atoms per formula unit: $(\text{Fe}_{2.23}\text{Ni}_{0.76})_{2.99}\text{P}_{1.01}$.

² Standard deviation. ³ Below detection limit (~ 0.05 wt.%).

4.2. Appearance and Physical Properties of Xenophyllite.

Xenophyllite forms elongated lamellar inclusions up to $20 \times 150 \mu\text{m}$ usually dissecting the encasing sarcopside grains (Figure 2). Xenophyllite lamellae are always confined to peripheral areas of sarcopside. Macroscopically, the mineral is translucent, has a bluish-green to grey-green color and vitreous lustre. Its powder color (the streak) is white. The Moh's hardness is 3.5–4. The lamellae are readily cleaved due to perfect cleavage on the $\{010\}$ plane. The density measured by sink-float of isolated grains in diluted Clerici solutions is $3.58(5) \text{ g/cm}^3$. The density calculated on the basis of empirical formula and the unit-cell parameters is $3.53(1) \text{ g/cm}^3$. In immersion liquids, xenophyllite is transparent and distinctly pleochroic, from yellow-green (X) to dark grey-green (Z). Due to crystal deformation, the mineral grains have undulatory extinction. Biaxial (–), $2V$ $10\text{--}20^\circ$, refractive indexes measured in Na-D light (589 nm): α 1.675(2), β 1.681(2), γ 1.681(2). The Gladstone-Dale compatibility index [17] calculated using a measured density is -0.010 (superior).

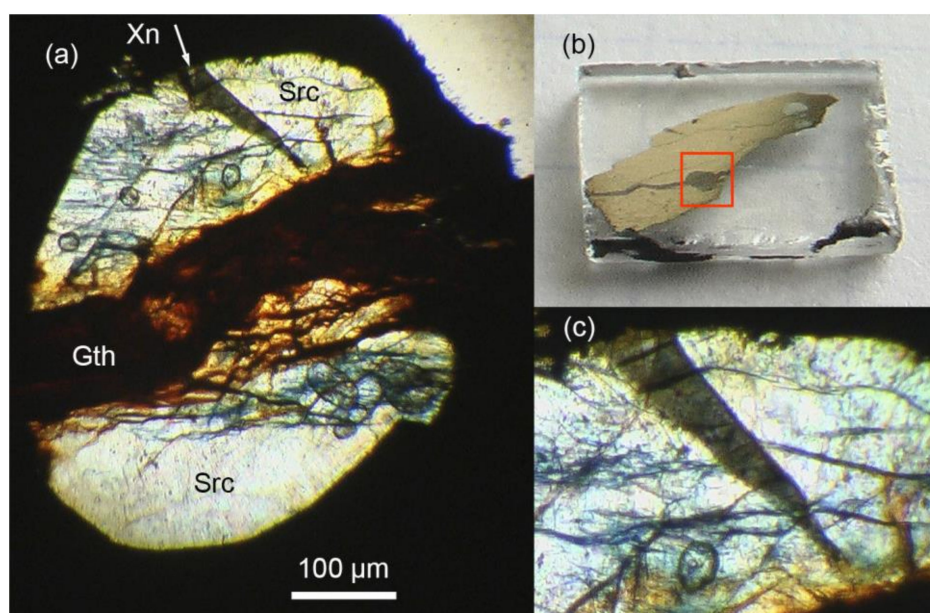


Figure 2. Xenophyllite in the Augustinovka meteorite. (a) A $\sim 0.5 \text{ mm}$ sarcopside grain cross-cut by secondary goethite and dissected with the green-grey xenophyllite lamella. Photomicrograph in transmitted light. (b) General view of troilite thin section containing phosphate assemblage depicted in Figure 1a (the field is outlined by the red square). (c) An enlarged view of xenophyllite lamella shown in Figure 1a. Photomicrograph in transmitted light. Abbreviations: Xn, xenophyllite; Src, sarcopside; Gth, goethite. Photographs by Sergey Britvin.

4.3. Single-Crystal Study and Powder X-Ray Diffraction

Xenophyllite crystals are substantially curved and twinned on (111) (in triclinic setting). That results in severe X-ray reflection overlapping and precludes obtaining the single-crystal data suitable for the structure refinement. However, the unit cell of the mineral could be determined and refined, and resulted in triclinic symmetry, space group *P*1 or *P*-1, with the parameters: *a* 9.643(6), *b* 9.633(5), *c* 17.645(11) Å; α 88.26(5), β 88.16(5), γ 64.83(5)°, *V* 1482(2) Å³, *Z* = 3. The refinement of the X-ray powder diffraction pattern (Table 3) using the single-crystal parameters as an input had led to the following cell metrics: *a* 9.617(4), *b* 9.608(4), *c* 17.649(13) Å; α 88.28(9), β 87.58(6), γ 64.92(3)°, *V* 1475.6(11) Å³, *Z* = 3.

Table 3. Powder X-ray diffraction data for xenophyllite (indexed in triclinic cell) (*d* in Å).

<i>I</i> _{meas}	<i>d</i> _{meas}	<i>d</i> _{calc}	<i>h</i>	<i>k</i>	<i>l</i>	<i>I</i> _{meas}	<i>d</i> _{meas}	<i>d</i> _{calc}	<i>h</i>	<i>k</i>	<i>l</i>
32	7.47	7.49	1	1	1	12	1.755	1.757	4	1	7
56	5.860	5.877	0	0	3			1.756	3	5	4
		5.843	−1	−1	2			1.754	5	4	2
4	4.964	4.967	1	−1	1			1.754	−4	−3	6
12	4.789	4.799	−1	0	3	8	1.732	1.733	0	1	10
		4.787	2	1	0			1.731	1	5	4
		4.785	1	2	0	6	1.646	1.646	−4	2	2
10	3.908	3.913	−2	−2	1			1.646	−4	−3	7
		3.911	0	−1	4			1.645	−3	3	3
		3.899	1	−1	3	6	1.639	1.640	5	2	6
22	3.319	3.317	2	−1	1			1.640	−3	−1	9
		3.315	2	1	4			1.639	1	−3	8
47	3.188	3.191	−1	−2	4			1.639	−3	−5	5
		3.187	3	1	0			1.638	5	0	4
		3.186	1	3	0	3	1.607	1.608	−5	−5	1
		3.184	−1	−1	5			1.606	5	5	2
100	3.020	3.024	−3	−2	1	8	1.594	1.594	6	2	0
		3.022	1	3	2			1.593	3	6	1
14	2.919	2.922	1	−2	3			1.593	2	−3	7
		2.921	−2	−2	4			1.593	−4	1	6
		2.917	−1	2	3			1.593	6	2	1
19	2.856	2.856	0	−3	1			1.593	2	6	0
14	2.813	2.812	1	0	6	10	1.559	1.560	−1	−1	11
67	2.719	2.722	0	−2	5			1.560	−1	−5	6
		2.718	2	2	5			1.560	−4	−5	5
77	2.703	2.701	3	3	0			1.559	−1	5	2
		2.701	2	−1	4			1.559	5	2	7
39	2.568	2.569	−3	0	3			1.559	0	4	8
		2.566	1	−1	6			1.558	−6	−3	2
18	2.534	2.534	−3	−1	4			1.558	−5	−4	5
31	2.395	2.396	1	3	5	4	1.533	1.534	−1	4	7
		2.394	4	2	0			1.534	−1	3	9
		2.393	2	4	0			1.533	4	6	2
10	2.345	2.345	1	4	1	6	1.518	1.519	6	2	4
8	2.104	2.106	0	−4	2			1.518	−5	1	3
		2.104	−1	−1	8	4	1.503	1.503	−3	−2	10
6	1.944	1.943	3	−2	3			1.503	5	−1	4
		1.942	4	3	5	5	1.445	1.446	−1	2	11
		1.942	−4	−2	5			1.446	0	−1	12
10	1.867	1.869	3	−2	4			1.446	5	5	6
		1.868	−3	−5	1			1.445	2	3	11
		1.867	−5	−3	1			1.445	−1	−6	4
		1.866	5	1	0			1.444	−4	3	2
10	1.773	1.774	5	4	0	4	1.408	1.408	−3	−5	8
		1.774	4	2	7						
		1.774	4	5	0						
		1.773	−5	−3	3						
		1.773	5	4	1						
		1.772	4	5	1						

The examination of the X-ray single-crystal dataset allowed to reveal two smaller subcells (monoclinic and orthorhombic) having the volumes equal to 2/3 of the triclinic cell volume (Table 4). The powder diffraction pattern of xenophyllite closely resembles that of galileiite, $\text{NaFe}_4(\text{PO}_4)_3$ [18], another rare Na-Fe phosphate also encountered in the IIIAB-group meteorites in the mineral assemblages similar to those of Augustinovka. The unit-cell parameters of xenophyllite are almost identical to those of its synthetic analogue reported by Pu et al. [5].

Table 4. The relationships between true triclinic cell of xenophyllite, the unit cell of its synthetic analogue and two xenophyllite subcells.

	Xenophyllite (the True Cell)	Synthetic $\text{Na}_4\text{Fe}_7(\text{PO}_4)_6$	Xenophyllite C-Centered Subcell	Xenophyllite I-Centered Subcell
Crystal system	Triclinic	Triclinic	Monoclinic	Orthorhombic
Space group	$P1$ or $P-1$	$P1$ or $P-1$	$C2/m$ or Cm	$Imma$ or $Im2a$
a (Å)	9.643(6)	9.647	16.257(9)	10.298(9)
b (Å)	9.633(5)	9.553	10.318(8)	14.997(7)
c (Å)	17.645(11)	17.573	6.257(9)	6.351(7)
α (°)	88.26(5)	88.43		
β (°)	88.16(5)	88.03	112.77(9)	
γ (°)	64.83(5)	64.80		
V (Å ³)	1482(2)	1464	968(2)	981(2)
Z	3	3	2	2
V/Z (Å ³)	494	488	484	491
T^1			$(\frac{1}{2}, -\frac{1}{2}, 0)(\frac{1}{2}, \frac{1}{2}, 0)(\frac{1}{2}, 0, 3)$	$(-\frac{1}{2}, \frac{1}{2}, \frac{1}{2})(\frac{1}{2}, \frac{1}{2}, \frac{1}{2})(0, \frac{1}{2}, -2.5)$
Reference	This work	[5] ²	This work	This work

¹ Transformation matrices to a triclinic cell. ² Reported as being refined by Rietveld method, but in fact it was refined by the Powley method (Supporting Information [5]).

4.4. Chemical Composition

Examination of several xenophyllite grains by means of an electron microprobe (Table 5) had revealed some distinctive features related to sodium contents in its composition. It was found that sodium is readily burned off from xenophyllite grains even under relatively soft analytical conditions. In particular, a 30 s exposure at 2 nA beam current and 1 μm beam diameter led to a loss of about one third of total sodium. In order to eliminate this effect, we used 1 nA beam current and 3 μm beam diameter. At these conditions, the loss of sodium was negligible; however, the accuracy of element determination was intentionally reduced to the first decimal (Table 5). The chemical composition of the type xenophyllite can be represented by the following empirical formula (based on 24 oxygen atoms per formula unit): $(\text{Na}_{3.67}\text{K}_{0.09})_{\Sigma 3.76}(\text{Fe}^{2+}_{6.12}\text{Mn}^{2+}_{0.85}\text{Cr}_{0.11})_{\Sigma 7.08}\text{P}_{5.99}\text{O}_{24.00}$. The latter one corresponds to the $\text{Na}_4\text{Fe}_7(\text{PO}_4)_6$ end-member. However, it was found that sodium contents in xenophyllite may considerably vary from grain to grain, ranging from $\text{Na}_4\text{Fe}_7(\text{PO}_4)_6$ to nearly $\text{Na}_2\text{Fe}_8(\text{PO}_4)_6 \equiv \text{NaFe}_4(\text{PO}_4)_3$. The latter formula, in due course, corresponds to a composition of galileiite [18], the mineral mentioned in the preceding section. Moreover, plotting the $(\text{Fe}, \text{MnCr})/(\text{Na}, \text{K}, \text{Ca})$ ratios determined for a series of xenophyllite grains reveals a remarkably straight, linear dependence between Na- and Fe-group elements which inspires the existence of continuous solid solutions between $\text{Na}_4\text{Fe}_7(\text{PO}_4)_6$ and $\text{Na}_2\text{Fe}_8(\text{PO}_4)_6$ end-members (Figure 3). The minerals of similar intermediate composition were reported from the eutectic chondritic melts described in Yanzhuang (H6) and Chelyabinsk (LL5) ordinary chondrites [19–21].

Table 5. Chemical composition of xenophyllite from the Augustinovka meteorite (analyses 1–8, our data) and galileiite from selected IIIAB iron meteorites (analyses A–D) ¹.

	Xenophyllite, wt.% ²								Galileiite, wt.% ²			
	1 ³	2	3	4	5	6	7	8	A	B	C	D
Na ₂ O	10.9	7.2	7.0	8.7	8.2	7.0	9.7	9.4	6.32	6.03	5.87	6.00
K ₂ O	0.4	bdl	bdl	bdl	bdl	bdl	bdl	bdl	1.07	0.26	0.04	0.01
CaO	bdl	0.1	bdl	bdl	bdl	bdl	0.4	0.2	0.01	bdl	bdl	0.02
FeO	42.1	46.4	42.4	44.3	40.1	48.5	43.1	41.0	43.47	51.67	48.95	34.63
MnO	5.8	6.1	9.7	7.0	11.7	5.8	5.8	7.5	5.42	1.87	3.98	16.98
MgO	bdl	bdl	0.2	bdl	bdl	bdl	0.2	bdl	bdl	bdl	bdl	bdl
Cr ₂ O ₃	0.8	0.5	1.0	0.6	1.4	bdl	0.6	1.2	1.55	0.13	0.07	1.16
P ₂ O ₅	40.7	39.1	39.5	40.3	39.2	38.7	40.3	40.7	41.19	39.61	40.25	43.99
Total	100.7	99.4	99.8	100.9	100.6	100.0	100.1	100.0	99.03	99.57	99.16	102.79
Atomic amounts (atoms per formula unit, recalculated to 24 oxygen atoms)												
Na	3.67	2.49	2.40	2.95	2.81	2.43	3.29	3.18	2.15	2.08	2.02	1.94
K	0.09	- ⁴	-	-	-	-	-	-	0.24	0.06	0.01	-
Ca	-	0.02	-	-	-	-	0.08	0.04	-	-	-	-
ΣNa	3.76	2.51	2.40	2.95	2.81	2.43	3.37	3.22	2.39	2.14	2.03	1.95
Fe	6.12	6.93	6.28	6.47	5.92	7.26	6.31	5.98	6.38	7.69	7.26	4.84
Mn	0.85	0.92	1.45	1.04	1.75	0.88	0.86	1.11	0.81	0.28	0.60	2.40
Mg	-	-	0.05	-	-	-	0.05	-	-	-	-	-
Cr	0.11	0.07	0.14	0.08	0.20	-	0.08	0.17	0.22	0.02	0.01	0.15
Σfe	7.09	7.92	7.93	7.59	7.86	8.13	7.31	7.26	7.40	7.99	7.87	7.39
P	5.99	5.91	5.92	5.96	5.86	5.86	5.97	6.01	6.12	5.97	6.04	6.22

¹ Galileiite [11]: A, Bear Creek; B, Bella Roca; C, Grant; D, Mount Edith. ² bdl: below detection limit. ³ The holotype specimen. ⁴ “-” means not detected.

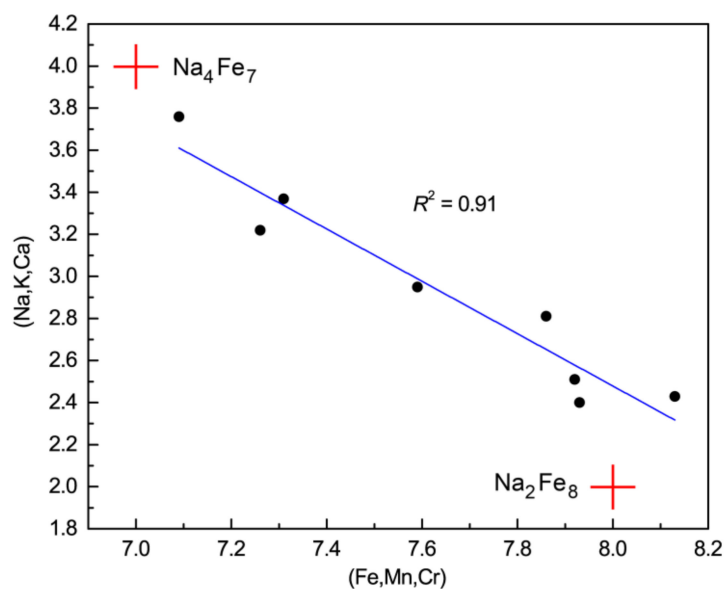


Figure 3. Variations of $\Sigma(\text{Na,K,Ca})$ vs. $\Sigma(\text{Fe,Mn,Cr})$ in the analyzed xenophyllite grains from the Augustinovka meteorite. Data in the atoms per formula unit (apfu) recalculated on 24 oxygen atoms. Red crosses denote the positions corresponding to ideal $\text{Na}_4\text{Fe}_7(\text{PO}_4)_6$ (top left) and $\text{Na}_2\text{Fe}_8(\text{PO}_4)_6$ (bottom right). The compositions are listed in Table 5.

4.5. Raman Spectroscopy

The Raman spectrum of xenophyllite was recorded at a reduced (to ~1 mW on sample) laser power and is depicted in Figure 4. The quality of the spectrum was degraded due to a strong concurrent fluorescence effect, hence only four main Raman bands could be reliably measured. The bands at 975

and 1114 cm^{-1} lie in the region typical of stretching modes of $[\text{PO}_4]^{3-}$ tetrahedra; their frequencies are close to the frequencies of galileiite-like phosphates reported from the ordinary chondrites [20]. The bands at 600 and 641 cm^{-1} are attributed to bending vibrations of orthophosphate anion and are distinguished from the bands reported for galileiite-like minerals from chondrites [20].

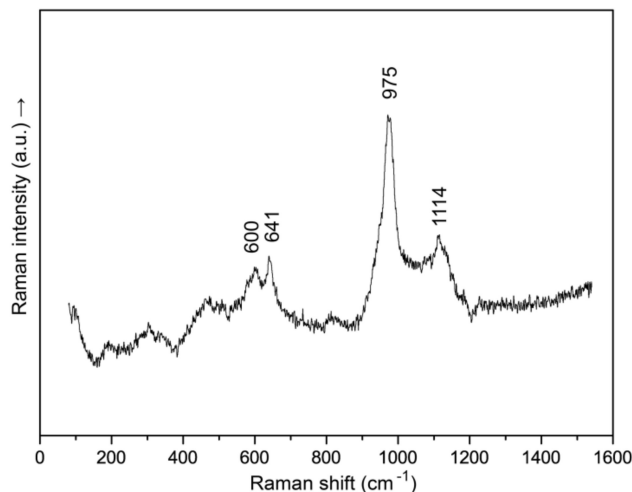


Figure 4. The Raman spectrum of xenophyllite (analysis 1 in Table 5).

5. Discussion

5.1. Relationships between Xenophyllite, Synthetic $\text{Na}_4\text{Fe}_7(\text{PO}_4)_6$ and $\text{ANa}_3\text{M}_7(\text{PO}_4)_6$ Phosphates

The recently reported characterization of a synthetic analogue of xenophyllite [5] had confirmed our previous data [6] on the symmetry (Table 4) and composition of the mineral. In spite of that, the structural relationships between xenophyllite and other phosphates were not yet defined. Herein we provide a comparison of xenophyllite, $\text{Na}_4\text{Fe}_7(\text{PO}_4)_6$, with a series of synthetic phosphates $\text{ANa}_3\text{M}_7(\text{PO}_4)_6$ ($A = \text{K}, \text{Rb}, \text{Cs}$; $M = \text{Mg}, \text{Fe}^{2+}, \text{Mn}^{2+}, \text{Zn}, \text{Co}^{2+}$) (Table 6). The first member of the family, $\text{CsNa}_3\text{Zn}_7(\text{PO}_4)_6$, was described by Yakubovich with co-authors [22]. Later on, nine compounds of Fe, Mn and Co were synthesized and studied with respect to their unusual magnetic properties [23,24]. The last reported phosphate of a series, $\text{RbNa}_3\text{Mg}_7(\text{PO}_4)_6$, was found to be a promising host matrix for the development of luminophore materials [25,26]. A series of structurally similar phosphates and arsenates was also reported, many of them being Na-ion conductors [27–33].

Table 6. Comparison of a monoclinic subcell of xenophyllite with the unit cells of representative $\text{ANa}_3\text{M}_7(\text{PO}_4)_6$ phosphates.

Compound	Space Group	<i>a</i> (Å)	<i>b</i> (Å)	<i>c</i> (Å)	β (°)	<i>V</i> (Å ³)	<i>Z</i>	<i>V/Z</i>	Reference
Xenophyllite	<i>A2/m</i> or <i>Am</i> ¹	12.514/2	10.318	16.257	112.77	968	2	484	This work
$\text{RbNa}_3\text{Mg}_7(\text{PO}_4)_6$	<i>C2/c</i>	12.734	10.685	15.498	112.83	1944	4	486	[25]
$\text{KNa}_3\text{Fe}_7(\text{PO}_4)_6$	<i>C2/c</i>	13.003	10.762	15.708	113.64	2013	4	503	[23]
$\text{KNa}_3\text{Mn}_7(\text{PO}_4)_6$	<i>C2/c</i>	13.165	10.907	15.960	113.24	2106	4	527	[24]
$\text{CsNa}_3\text{Zn}_7(\text{PO}_4)_6$	<i>C2/c</i>	13.151	10.901	15.994	113.20	2107	4	527	[22]

¹ Xenophyllite subcell was transformed to *cba*-setting for a better comparability with other compounds.

The cell metrics of a monoclinic subcell of xenophyllite is obviously related to the unit cells of $\text{ANa}_3\text{M}_7(\text{PO}_4)_6$ phosphates (Table 6), distinguishing from them just by a doubly reduced *c*-axis. That is, together with the same stoichiometry, it strongly suggests structural relationships between xenophyllite and these phosphates. It should be noted that the above compounds possess unique channel-like structures not encountered among natural phosphates. That is, in due course, this largely eliminates speculation about the possible relation of xenophyllite to fawcittite-group minerals [34].

5.2. Xenophyllite and Galileiite

Galileiite, $\text{NaFe}_4(\text{PO}_4)_3$, was described from several iron meteorites [18] (Table 5) which, like the Augustinovka, belong to a structural group of medium octahedrites and a chemical group IIIAB. The mineral assemblages of galileiite [12,18] are almost identical to those of xenophyllite from the Augustinovka. The analytical abilities did not allow the X-ray single-crystal data for galileiite to be obtained. The powder diffraction pattern of the mineral (Gandolfi method) was reported and was indexed assuming the possible relationship of galileiite to fillowite-group minerals [18]. However, the authors note that the indexing in rhombohedral (fillowite) cell [34] was not entirely satisfactory, and the assertion of galileiite as a mineral belonging to the fillowite group “is yet to be demonstrated” [18]. What is more interesting is that the cell metrics of an *I*-centered subcell of xenophyllite almost exactly reproduces the unit-cells of a wide series of synthetic phosphates $\text{AM}_{3-4}(\text{PO}_4)_3$ having the stoichiometry of galileiite, $\text{NaFe}_4(\text{PO}_4)_3$ (Table 7). In particular, the “potassium analog of galileiite” [18] has a direct synthetic $\text{KFe}_4(\text{PO}_4)_3$ counterpart [34]. The crystal structures of these phosphates are very similar to each other and do not belong to a fillowite structure [35]. Instead, they have tunnel-like architectures derivative of the $\alpha\text{-CrPO}_4$ structure type [36]. Many of those phosphates have ion-conductive properties [37].

Table 7. Comparison of *I*-centered subcell of xenophyllite with the unit cells of galileiite-like synthetic phosphates.

Compound	Space Group	<i>a</i> (Å)	<i>b</i> (Å)	<i>c</i> (Å)	<i>V</i> (Å ³)	Reference
Xenophyllite	<i>Imma</i> ¹	10.298	14.997	6.351	981	This work
$\text{SrFe}_3(\text{PO}_4)_3$	<i>Imma</i>	10.438	13.421	6.556	919	[38]
$\text{NaNi}_4(\text{PO}_4)_3$	<i>Amam</i> ²	9.892	14.842	6.358	933	[39]
$\text{NaMg}_4(\text{PO}_4)_3$	<i>Pnma</i>	9.883	6.345	15.240	956	[40]
$\text{KMn}_4(\text{PO}_4)_3$	<i>Pmcn</i> ²	6.550	16.028	9.977	1047	[41]
$\text{NaCo}_4(\text{PO}_4)_3$	<i>P2₁/n</i>	6.339	9.867	15.300	957 ³	[42]
$\text{KFe}_4(\text{PO}_4)_3$	<i>Pmnn</i>	6.273	16.513	9.808	1016	[34]
$\text{KMg}_4(\text{PO}_4)_3$	<i>Pnnm</i>	16.361	9.562	6.171	966	[43]
$\text{KNi}_4(\text{PO}_4)_3$	<i>Pmnn</i>	6.152	16.214	9.484	946	[42]

¹*I*-centered subcell, alternative space group *Imm2*. ² Alternative solution: *Pmnn* [44]. ³ $\beta = 91.05^\circ$.

Taking into account the evidence available to date, one can state that there are many similarities between these two minerals. First, note the numerous overlaps between the strong X-ray powder diffraction lines of xenophyllite (Table 4) and galileiite [18]. Second, our electron microprobe data evidence for the occurrence of a continuous series of compounds between $\text{Na}_4\text{Fe}_7(\text{PO}_4)_6$ and $\text{Na}_2\text{Fe}_8(\text{PO}_4)_6$ [$\equiv \text{NaFe}_4(\text{PO}_4)_3$] (Table 5, Figure 3). Note that Olsen & Steele [18] have used relatively harsh analytical conditions during the microprobe examination of galileiite (WDX system, 15 kV, 25 nA) that could result in a considerable loss of sodium during their analyses. However, our measurements were carried out with a great care under the soft conditions (*cf.* Materials and Methods section), therefore we can confirm that the galileiite-type $\text{NaFe}_4(\text{PO}_4)_3$ is a mineral rather than an artifact produced by the overburning of Na-rich xenophyllite under the hard electron beam. The occurrence of phosphates having intermediate xenophyllite-galileiite composition was also reported later on from a series of ordinary chondrites [19–21,45,46], anomalous meteorite Sahara 03505 [47] and from burned coal piles [48,49].

6. Conclusions

Xenophyllite, being discovered as a rare mineralogical curiosity [6], has become a natural prototype of synthetic $\text{Na}_4\text{Fe}_7(\text{PO}_4)_6$, a new material with promising electrochemical properties [5]. The sodium ions mobility first revealed during electron microprobe measurements of the mineral has met its electrochemical implications. The close relationships between xenophyllite and a series of synthetic phosphates (Tables 6 and 7) might suggest that the latter compounds bearing redox-sensitive cations

Fe^{2+} , Mn^{2+} and Co^{2+} have to be explored for their applicability as materials for Na-ion batteries. Further structural studies are needed to reveal the exact mechanisms of Na-ions mobility in xenophyllite and the obvious relationships with its nearest mineralogical counterpart, galileiite.

Supplementary Materials: The following are available online at <http://www.mdpi.com/2075-163X/10/4/300/s1>, Figure S1: As-recorded imaging plate pattern of xenophyllite. Rigaku RAXIS Rapid II diffractometer, semi-cylindrical imaging plate, $\text{CoK}\alpha$ -radiation (rotating anode with microfocus optics), 40 kV acceleration voltage, 15 mA tube current, 127.4 mm detector-to-crystal distance, 60 min exposure time. The black rectangle outlines the area used for the integration of imaging plate data into an XRD profile., Figure S2: Powder XRD profile of xenophyllite obtained by integration of imaging plate data shown in Figure S1.

Author Contributions: Conceptualization, methodology and writing, S.N.B.; X-ray studies, S.V.K. and S.N.B.; electron microprobe study, N.S.V.; Raman spectroscopy, V.N.B.; samples preparation, E.V.O. and V.V.B. All authors have read and agreed to the published version of the manuscript.

Funding: This research was funded by Russian Science Foundation, grant number 18-17-00079.

Acknowledgments: We gratefully thank the curators of the Mining Museum, Saint Petersburg Mining University, for loaning the specimens of the Augustinovka meteorite used in this study. The editors and anonymous reviewers are thanked for handling and careful examination of the manuscript. The authors thank the X-ray Diffraction Centre, Geomodel Resource Centre and Interdisciplinary Resource Centre of Nanotechnology of Saint Petersburg State University for providing instrumental and computational resources.

Conflicts of Interest: The authors declare no conflicts of interest.

References

1. Yakubovich, O.V.; Simonov, M.A.; Belov, N.V. The crystal structure of a synthetic triphylite $\text{LiFe}(\text{PO}_4)$. *Sov. Phys. Dokl.* **1977**, *22*, 347–348.
2. Padhi, A.K.; Nanjundaswamy, K.S.; Goodenough, J.B. Phospho olivines as Positive Electrode Materials for Rechargeable Lithium Batteries. *J. Electrochem. Soc.* **1997**, *144*, 1188–1194. [[CrossRef](#)]
3. Fergus, J.W. Recent developments in cathode materials for lithium ion batteries. *J. Power Sources* **2010**, *195*, 939–954. [[CrossRef](#)]
4. Jamesh, M.I.; Prakash, A.S. Advancement of technology towards developing Na-ion batteries. *J. Power Sources* **2018**, *378*, 268–300. [[CrossRef](#)]
5. Pu, X.; Rong, C.; Tang, S.; Cao, S.; Wang, H.; Ding, Y.; Cao, Y.; Chen, Z. Zero-strain $\text{Na}_4\text{Fe}_7(\text{PO}_4)_6$ as a novel cathode material for sodium-ion batteries. *Chem. Commun.* **2019**, *55*, 9043–9046. [[CrossRef](#)] [[PubMed](#)]
6. Britvin, S.N. *New Minerals Approved in 2006. Nomenclature Modifications Approved in 2006 by the Commission on New Minerals, Nomenclature and Classification*; Burke, E.A.J., Ferraris, G., Hatert, F., Eds.; International Mineralogical Association: Paris, France, 2006. Available online: <http://cnmnc.main.jp/minerals2006.pdf> (accessed on 25 February 2020).
7. Alexeev, W. Ueber den Meteorit aus dem Dorfe Awgustinowka, Gouvernement Jekaterinoslaw. *Proc. Russ. Miner. Soc.* **1893**, *30*, 475.
8. Meunier, M.S. Sur le météorique d'Augustinowka (Russie). *Compt. Rend. Acad. Sci.* **1893**, *116*, 1151–1153.
9. Buchwald, V.F. *Handbook of Iron Meteorites*; University of California Press: Berkeley, CA, USA, 1975; Volume 2, pp. 279–281.
10. The Augustinovka meteorite. Available online: <https://webmineral.ru/minerals/image.php?id=12970> (accessed on 25 February 2020).
11. Olsen, E.; Fredriksson, K. Phosphates in iron and pallasite meteorites. *Geochim. Cosmochim. Acta* **1966**, *30*, 459–470. [[CrossRef](#)]
12. Olsen, E.J.; Kracher, A.; Davis, A.M.; Steele, I.M.; Hutcheon, I.D.; Bunch, T.E. The phosphates of IIIAB iron meteorites. *Meteorit. Planet. Sci.* **1999**, *34*, 285–300. [[CrossRef](#)]
13. Pieczka, A.; Hawthorne, F.C.; Ball, N.; Abdu, Y.; Gołębiewska, B.; Włodek, A.; Żukrowski, J. Graftonite-(Mn), ideally $\text{M}^1\text{Mn}^{\text{M}^2\text{M}^3}\text{Fe}_2(\text{PO}_4)_2$, and graftonite-(Ca), ideally $\text{M}^1\text{Ca}^{\text{M}^2\text{M}^3}\text{Fe}_2(\text{PO}_4)_2$, two new minerals of the graftonite group from Poland. *Miner. Mag.* **2018**, *82*, 1307–1322. [[CrossRef](#)]
14. X-AREA, Version 1.42; Stoe & Cie GmbH: Darmstadt, Germany, 2007.
15. Britvin, S.N.; Dolivo-Dobrovolsky, D.V.; Krzhizhanovskaya, M.G. Software for processing the X-ray powder diffraction data obtained from the curved image plate detector of Rigaku RAXIS Rapid II diffractometer. *Proc. Russ. Miner. Soc.* **2017**, *146*, 104–107.

16. Stoe and Cie GmbH. *STOE WinXPOW (Version 1.06)*; Stoe and Cie GmbH: Darmstadt, Germany, 1999.
17. Mandarino, J.A. The Gladstone-Dale relationship. Part IV. The compatibility concept and its application. *Can. Miner.* **1981**, *19*, 441–450.
18. Olsen, E.J.; Steele, I.M. Galileiite: A new meteoritic phosphate mineral. *Meteorit. Planet. Sci.* **1997**, *32*, A155–A156. [[CrossRef](#)]
19. Chen, M.; Xie, X. Na behavior in shock-induced melt phase of the Yanzhuang (H6) chondrite. *Eur. J. Miner.* **1996**, *8*, 325–333.
20. Xie, X.; Chen, M.; Zhai, S.; Wang, F. Eutectic metal + troilite + Fe-Mn-Na phosphate + Al-free chromite assemblage in shock-produced chondritic melt of the Yanzhuang chondrite. *Meteorit. Planet. Sci.* **2014**, *49*, 2290–2304. [[CrossRef](#)]
21. Sharygin, V.V.; Karmanov, N.S.; Podgornyykh, N.M. Na-Fe-Phosphate Globules in Impact Metal-Troilite Associations of Chelyabinsk Meteorite. In Proceedings of the 79th Annual Meeting of the Meteoritical Society, Berlin, Germany, 7–12 August 2016.
22. Yakubovich, O.V.; Mel'nikov, O.K.; Urusov, V.S.; Massa, V.; Vochadlo, S. Crystal structure of a new orthophosphate $\text{CsNa}_3\text{Zn}_7(\text{PO}_4)_6$. *Doklady Akademii Nauk-Rossiyskaya Akademiya Nauk* **1996**, *348*, 755–758.
23. Queen, W.L.; Hwu, S.-J.; Wang, L. A Low-Dimensional Iron(II) Phosphate Exhibiting Field-Dependent Magnetization Steps. *Angew. Chem. Int. Ed.* **2007**, *46*, 5344–5347. [[CrossRef](#)]
24. Guo, W.; He, Z.; Zhang, S.; Yang, M.; Tang, Y.; Cheng, W. $\text{KNa}_3\text{Mn}_7(\text{PO}_4)_6$: 2D spin-frustrated magnetic material with a diamond-like chain structure. *RSC Adv.* **2014**, *4*, 21559–21562. [[CrossRef](#)]
25. Ben Hamed, T.; Boukhris, A.; Badri, A.; Ben Amara, M. Synthesis and crystal structure of a new magnesium phosphate $\text{Na}_3\text{RbMg}_7(\text{PO}_4)_6$. *Acta Cryst. E* **2017**, *73*, 817–820. [[CrossRef](#)]
26. Böhnisch, D.; Rosenboom, J.; García-Fuente, A.; Urland, W.; Jüstel, T.; Baur, F. On the Blue Emitting Phosphor $\text{Na}_3\text{RbMg}_7(\text{PO}_4)_6:\text{Eu}^{2+}$ Showing Ultra High Thermal Stability. *J. Mater. Chem. C* **2019**, *7*, 6012–6021. [[CrossRef](#)]
27. Moring, J.; Kostiner, E. The crystal structure of $\text{Na}_4\text{Ni}_7(\text{PO}_4)_6$. *J. Solid State Chem.* **1986**, *62*, 105–111. [[CrossRef](#)]
28. Kobashi, D.; Kohara, S.; Yamakawa, J.; Kawahara, A. Un monophosphate synthétique de sodium et de cobalt: $\text{Na}_4\text{Co}_7(\text{PO}_4)_6$. *Acta Cryst. C* **1998**, *54*, 7–9. [[CrossRef](#)]
29. Ben Smail, R.; Driss, A.; Jouini, T. $\text{K}_4\text{Ni}_7(\text{AsO}_4)_6$. *Acta Cryst. C* **1999**, *55*, 284–286. [[CrossRef](#)]
30. Marzouki, R.; Frigui, W.; Guesmi, A.; Zid, M.F.; Driss, A. β -Xenophyllite-type $\text{Na}_4\text{Li}_{0.62}\text{Co}_{0.567}\text{Al}_{0.71}(\text{AsO}_4)_6$. *Acta Cryst.* **2013**, *69*, i65–i66. [[CrossRef](#)] [[PubMed](#)]
31. Ben Smida, Y.; Marzouki, R.; Georges, S.; Kutteh, R.; Avdeev, M.; Guesmi, A.; Zid, M.F. Synthesis, crystal structure, electrical properties, and sodium transport pathways of the new arsenate $\text{Na}_4\text{Co}_7(\text{AsO}_4)_6$. *J. Solid State Chem.* **2016**, *239*, 8–16. [[CrossRef](#)]
32. Issaoui, C.; Chebbi, H.; Guesmia, A. Crystal structure of $\text{Na}_4\text{Co}_7-x\text{Al}_{0.67x}(\text{As}_{1-y}\text{PyO}_4)_6$ ($x = 1.60$; $y = 0.116$). *Acta Cryst.* **2016**, *72*, 495–497. [[CrossRef](#)] [[PubMed](#)]
33. Marzouki, R. Electrical properties and alkali-pathways simulation of new mixed conductor $\text{Na}_4\text{Li}_{0.62}\text{Co}_{0.567}\text{Al}_{0.71}(\text{AsO}_4)_6$. *Mater. Res. Exp.* **2020**, *7*, 016313. [[CrossRef](#)]
34. Matvienko, E.N.; Yakubovich, O.V.; Simonov, M.A.; Belov, N.V. The crystal structure of K, Fe-orthophosphate $\text{KFe}_4(\text{PO}_4)_3$. *Doklady Akademii Nauk SSSR* **1981**, *259*, 591–595.
35. Moore, P.B. Perception of structural complexity: Fillowite revisited and α -iron related. *Am. Miner.* **1989**, *74*, 918–1926.
36. Attfield, J.P.; Cheetham, A.K.; Cox, D.E.; Sleight, A.W. Synchrotron X-ray and Neutron Powder Diffraction Studies of the Structure of α - CrPO_4 . *J. Appl. Cryst.* **1988**, *21*, 452–457. [[CrossRef](#)]
37. Daidouh, A.; Pico, C.; Veiga, M.L. Structure features and ionic conductivity of the $\text{AM}_4(\text{PO}_4)_3$ orthophosphates: ($A = \text{Na, K, Rb}$; $M = \text{Ni, Mn}$). *Solid State Ion.* **1999**, *124*, 109–117. [[CrossRef](#)]
38. Chen, Y. Mild hydrothermal synthesis and structures of mixed-valence iron phosphates: $\text{SrFe}_3(\text{PO}_4)_3$ and the interesting Mg^{2+} -doped $\text{AFe}_3(\text{PO}_4)_3$ ($A = \text{Ba, Pb}$) in Fe^{2+} site. *Cryst. Res. Technol.* **2012**, *47*, 1185–1189. [[CrossRef](#)]
39. Anderson, J.B.; Moring, J.; Kostiner, E. Disorder in the crystal structure of $\text{NaNi}_4(\text{PO}_4)_3$. *J. Solid State Chem.* **1985**, *60*, 358–365. [[CrossRef](#)]
40. Amara, M.B.; Vlasse, M.; Olazcuaga, R.; le Flem, G.; Hagenmuller, P. La structure de l'orthophosphate triple de magnesium et de sodium, $\text{NaMg}_4(\text{PO}_4)_3$. *Acta Cryst. C* **1983**, *39*, 936–939. [[CrossRef](#)]

41. Yakubovich, O.V.; Evdokimova, O.A.; Mel'nikov, O.K.; Simonov, M.A. Crystal structure of the new K, Mn²⁺ orthophosphate KMn₄(PO₄)₃. *Sov. Phys. Cryst.* **1986**, *31*, 151–154.
42. Baies, R.; Perez, O.; Caignaert, V.; Pralong, V.; Raveau, B. A new sodium cobaltophosphate with a tunnel structure, ionic conductor. *J. Mater. Chem.* **2006**, *16*, 2434–2438. [[CrossRef](#)]
43. Tomaszewski, P.E.; Maczka, M.; Majchrowski, A.; Waskowska, A.; Hanuza, J. Crystal structure and vibrational properties of KMg₄(PO₄)₃. *Solid State Sci.* **2005**, *7*, 1201–1208. [[CrossRef](#)]
44. Daidouh, A.; Martinez, J.L.; Pico, C.; Veiga, M.L. Structure characterization and magnetic behavior of NaNi₄(PO₄)₃ and KMn₄(PO₄)₃. *J. Solid State Chem.* **1999**, *144*, 169–174. [[CrossRef](#)]
45. Semenenko, V.P.; Perron, C. Shock-melted material in the Krymka LL3.1 chondrite: Behavior of the opaque minerals. *Meteorit. Planet. Sci.* **2005**, *40*, 173–185. [[CrossRef](#)]
46. Sharygin, V.V. Na-Fe-Phosphate Globules in Impact Metal-Sulfide Associations from Meteorite Chelyabinsk: Composition and Raman Spectroscopy. In Proceedings of the IV International conference “Meteorites. Asteroids. Comets”, Ekaterinburg, Russia, 26–28 May 2016.
47. D’Orazio, M.; Folco, L.; Chaussidon, M.; Rochette, P. Sahara 03505 sulfide-rich iron meteorite: Evidence for efficient segregation of sulfide-rich melt during high-degree impact melting of an ordinary chondrite. *Meteor. Planet. Sci.* **2009**, *44*, 221–231. [[CrossRef](#)]
48. Sharygin, V.V. Sarcopside from “black blocks” of the 45 mine burned dump, Kopeisk, Chelyabinsk coal basin. In Proceedings of the “Mineralogy of the Urals”, Miass-Ekaterinburg, Russia, 22–27 August 2011; pp. 183–186.
49. Sharygin, V.V. Phosphate Inclusions in Cohenite from “Black Blocks” of the 45 Mine Burned Dump, Kopeisk, Chelyabinsk Coal Basin. In Proceedings of the Mineralogy of Technogenesis, Miass, Russia, 23–26 June 2016; pp. 34–49.



© 2020 by the authors. Licensee MDPI, Basel, Switzerland. This article is an open access article distributed under the terms and conditions of the Creative Commons Attribution (CC BY) license (<http://creativecommons.org/licenses/by/4.0/>).